The Astrophysical Journal, 861:61 (12pp), 2018 July 1 https://doi.org/10.3847/1538-4357/aac826

Stability of CH_3NCO in Astronomical Ices under Energetic Processing: A Laboratory Study

B. Maté[1], G. Molpeceres[1], I. Tanarro[1], R. J. Peláez[1], J. C. Guillemin[2], J. Cernicharo[3], and V. J. Herrero[1]
[1] Instituto de Estructura de la Materia (IEM-CSIC), Serrano 121-123, E-28006 Madrid, Spain; v.herrero@csic.es
[2] Univ. Rennes, Ecole Nationale Supérieure de Chimie de Rennes, CNRS, ISCR—UMR6226, F-35000 Rennes, France
[3] Instituto de Física Fundamental (IFF-CSIC), Serrano 121-123, E-28006, Madrid, Spain
Received 2018 March 12; revised 2018 May 21; accepted 2018 May 23; published 2018 July 3

Abstract

Methyl isocyanate (CH_3NCO) was recently found in hot cores and suggested to exist on comet 67P/CG. The incorporation of this molecule into astrochemical networks requires data on its formation and destruction. In this work, ices of pure CH_3NCO and of $CH_3NCO(4\%–5\%)/H_2O$ mixtures deposited at 20 K were irradiated with a UV D_2 lamp (120–400 nm) and bombarded by 5 keV electrons to mimic the secondary electrons produced by cosmic rays (CRs). The destruction of CH_3NCO was studied using IR spectroscopy. After processing, the ν_a–NCO band of CH_3NCO disappeared and IR bands corresponding to CO, CO_2, OCN^-, and HCN/CN^- appeared instead. The products of photon and electron processing were very similar. Destruction cross sections and half-life doses were derived from the measurements. Water ice provides a good shield against UV irradiation (half-life dose of $\sim$64 eV molecule^{-1} for CH_3NCO in water ice), but is not so good against high-energy electrons (half-life dose $\sim$18 eV molecule^{-1}). It was also found that CH_3NCO does not react with H_2O over the temperature range 20–200 K. These results indicate that hypothetical CH_3NCO in the ices of dense clouds should be stable against UV photons and relatively stable against CRs over the lifetime of a cloud ($\sim10^7$ yr), and could sublime in the hot core phase. On the surface of a Kuiper Belt object (the original location of comet 67P/CG) the molecule would be swiftly destroyed, by both photons and CRs, but embedded below just 10 μm of water ice, the molecule could survive for $\sim10^9$ yr.

Key words: astrochemistry – interstellar medium (ISM) – Kuiper Belt: general – molecular data – solid state: volatile

1. Introduction

The analysis of mass spectrometric measurements from the Cometary Sampling and Composition (COSAC) instrument of *Rosetta*'s Philae lander (Goesmann et al. 2015) indicated that methyl isocyanate was abundant at the surface of comet 67P/Churyumov–Gerasimenko (CG). A ratio of $CH_3NCO/H_2O = 1.3\%$ was estimated from these measurements. The isocyanate functional group is structurally similar to a peptide bond, and chemical routes implying isocyanates have been invoked in models of peptide synthesis under prebiotic conditions (Pascal et al. 2005). In spite of its potential interest for prebiotic chemistry, methyl isocyanate was not included in astrochemical models before the publication of the COSAC results.

Soon after the publication of the work of Goesmann et al. (2015) the presence of CH_3NCO was also reported in the interstellar medium (ISM) (Halfen et al. 2015; Cernicharo et al. 2016). The line survey of Orion, carried out with the 30 m IRAM telescope (Tercero et al. 2010, 2012) motivated the complete characterization of CH_3NCO in the laboratory. Several groups were involved in this work (see Cernicharo et al. 2016 and references therein). Another group (Halfen et al. 2015) sought the molecule, motivated by its detection in comet 67P/CG. Methyl isocyanate was then detected in two high-mass protostars. Halfen et al. (2015) identified it in SgrB2(N) using data from the 12 m telescope of the Arizona Radio Observatory, and Cernicharo et al. (2016) found it in Orion KL with data from the 30 m IRAM telescope and from the Atacama Large Millimeter Array (ALMA). The analysis of the Orion KL measurements and a re-evaluation of previous SgrB2 data (Cernicharo et al. 2016) showed that the molecule was present in the warm gas of these clouds. Besides, Cernicharo et al. (2016) reported upper limits for the abundance of CH_3NCO in cold dark clouds and also for its isomers CH_3CNO and CH_3OCN, which were not detected towards the two high-mass protostars where CH_3NCO was initially discovered. Additional observations of methyl isocyanate in the SgrB2(N2) hot core were published by Belloche et al. (2017). More recently, Ligterink et al. (2017) and Martín-Doménech et al. (2017), using ALMA data, were able to identify CH_3NCO in the warm gas of the low-mass solar-type protostar IRAS 16293-2422. In the gas phase of the protostars, the proportion of CH_3NCO was found to be much smaller than that reported for the surface of comet 67P/CG. In Orion KL, for instance, a ratio of $CH_3NCO/H_2O = 0.02\%$ was derived by Cernicharo et al. (2016). Abundance ratios of CH_3NCO with respect to characteristic N-bearing species such as HNCO and CH_3CN are also much lower in the protostars (Cernicharo et al. 2016; Ligterink et al. 2017) than those reported by Goesmann et al. (2015) for the comet's surface. Although the presence of CH_3NCO in the ISM is well established at present, the original results from 67P/CG have been questioned. New data have recently been published by Altwegg et al. (2017). These authors could not identify CH_3NCO in the coma of the comet with the high-resolution Double Focusing Mass Spectrometer of the *Rosetta* Orbiter Spectrometer for Ion and Neutral Analysis (ROSINA). In the same work, the COSAC data were revisited and the presence of CH_3NCO could not be confirmed.

Gas-phase mechanisms leading to the production of CH_3NCO in the ISM were discussed by Halfen et al. (2015). They were based on reactions of HNCO or HOCN with either CH_3 or CH_5^+, but the gas-phase concentrations of HOCN, CH_3,

and CH_5^+ in the ISM are probably too low (see discussion in Ligterink et al. 2017). Most authors assume that reactions in the bulk or at the surface of the ice mantles covering dust grains are more probable formation pathways for CH_3NCO. Specifically, Cernicharo et al. (2016) have proposed the reaction

$$CH_3(s) + HNCO(s) \rightarrow CH_3NCO(s) + H(s) \quad (1)$$

and Belloche et al. (2017) the reaction

$$CH_3(s, g) + NCO(s) \rightarrow CH_3NCO(s) \quad (2)$$

where s and g stand for *solid* and *gas* respectively, as sources of CH_3NCO in interstellar ices. Experiments by Ligterink et al. (2017), based on the vacuum ultraviolet (VUV) irradiation of CH_4/HNCO mixtures at 20 K, suggest that the formation of methyl isocyanate through reactions (1) and (2) is indeed possible. The methyl isocyanate produced in the ices would sublimate with rising temperature in the evolution of the protostar, and that would explain its presence in hot cores (Halfen et al. 2015; Cernicharo et al. 2016; Belloche et al. 2017) and hot corinos (Ligterink et al. 2017; Martín-Doménech et al. 2017). The reactions mentioned in this paragraph have been incorporated into astrochemical models (Belloche et al. 2017; Martín-Doménech et al. 2017; Majumdar et al. 2018; Quénard et al. 2018) that provide a plausible explanation for the presence of CH_3NCO in the ISM, but quantitative predictions of column densities, allowing a direct comparison with observations, are difficult due to the absence of kinetic data and to the uncertainty about the concentration of the proposed chemical precursors of methyl isocyanate, both in the ices and in the gas phase.

The production of CH_3NCO by reactions (1) and (2) requires the presence of radicals within the ice. The experiments of Ligterink et al. (2017) show that UV photolysis of CH_4 could account for the formation of the necessary CH_3 radicals. Besides UV photons, cosmic rays (CRs) and thermal heating can induce chemistry in astrophysical ices by producing active species (atoms, radicals, or ions) in the solid medium (Allamandola et al. 1988; Moore et al. 2001; Baratta et al. 2002). However, energetic processing of ices has ambivalent effects. On the one hand it can trigger a chemistry leading to an increase in molecular complexity (Jamieson et al. 2006; Linnartz et al. 2011; Theulé et al. 2013; Öberg 2016), but on the other hand it can destroy complex structures. The occurrence of a given molecule in a particular environment will depend on the balance between these two effects.

In this work we study the destruction of CH_3NCO in ices under energetic processing. Ice samples of pure methyl isocyanate and of methyl isocyanate diluted in water ice are irradiated with UV photons and bombarded with high-energy (5 keV) electrons, which mimic the secondary electrons produced by CRs (Kaiser et al. 2013; Mason et al. 2014; Maté et al. 2015, 2016). The decay of the CH_3NCO concentration as a function of the energy doses absorbed is derived from these measurements, and the implications for the survival probability of CH_3NCO in interstellar and cometary ices are discussed.

2. Experiment

The set-up for the generation, processing, and infrared spectroscopy of ices has been described extensively elsewhere (Maté et al. 2003, 2014; Gálvez et al. 2007) and only the details relevant to this work are given here. It consists of a vacuum chamber with a closed-cycle He cryostat, whose cold finger holds an IR-transparent Si window where ices of the species of interest are condensed from the vapor phase. The temperature of the Si substrate can be varied between 14 K and 300 K with 1 K accuracy. The chamber is coupled through two KBr windows to a Vertex70 Fourier transform IR spectrometer configured for normally incident transmission. A rotatable flange allows the orientation under vacuum of the Si substrate, which in the course of the present experiments faced alternatively the IR beam of the spectrometer or a chamber port provided with a UV lamp or an electron gun. The spectra were recorded with a resolution of 2 cm^{-1} using an HgCdTe (MCT) detector refrigerated with liquid nitrogen. The gas-phase composition during deposition was monitored by means of a calibrated quadrupole mass spectrometer (QMS) placed in an adjacent chamber (Maté et al. 2017). The base pressure in the vacuum chamber was $\sim(0.7–1) \times 10^{-8}$ mbar. Methyl isocyanate was prepared with a modified version of the synthesis of Han et al. (1989). Silver cyanate (15.0 g, 0.1 mol), dry diethyleneglycol dibutyl ether (25 mL), and iodomethane (7.10 g, 50 mmol) were mixed together in a cell equipped with a magnetic stirring bar and a stopcock. The cell was immersed in a liquid nitrogen bath and degassed. The mixture was heated under stirring at 90°C for 20 hr. The cell was then fitted on a vacuum line (0.1 mbar) equipped with two traps and low boiling compounds were distilled. The first trap was immersed in a bath cooled at −30°C to remove high boiling compounds. The low boiling methyl isocyanate was selectively condensed in the second trap immersed in a liquid nitrogen bath. The yield was 40%. (Caution: methyl isocyanate is a highly toxic, severe lachrymatory agent and should be handled with care.)

Methyl isocyanate vapor was introduced to the chamber by means of a needle valve connecting the chamber with a small Pyrex flask containing approximately 5 ml of liquid methyl isocyanate. For a better handling of the vapor flow to the chamber, the flask was held in an ice bath or in a bath with ice and salt. The liquid samples were subjected to three freeze–pump–thaw cycles for degassing before allowing methyl isocyanate into the vacuum chamber. Deposits were formed at a substrate temperature of 20 K. Deposition pressures in the range $\approx 10^{-6}$ mbar and deposition times of several minutes were typically used. Ice mixtures of CH_3NCO and H_2O, with typical CH_3NCO/H_2O ratios in the range 4%–5%, were also co-deposited on the substrate. Separate entrances were used for the H_2O and CH_3NCO vapors, and the mixture proportion in the ices was estimated from the absorbance ratio of the most intense absorption bands of water: $A = 1.9 \times 10^{-16}$ cm molecule^{-1} for ν-OH (Mastrapa et al. 2009), and methyl isocyanate: $A = 1.3 \times 10^{-16}$ cm molecule^{-1} for ν_a–NCO (Maté et al. 2017).

The deposited CH_3NCO and CH_3NCO/H_2O samples were processed with UV photons and high-energy electrons. A D_2 lamp, Hamamatsu L10706, was used for the UV irradiation measurements. The spectral range of the lamp goes from 120 to 400 nm with most of the emission concentrated at wavelengths <180 nm. In the following we will focus on the range 120–180 nm (10.3–6.9 eV) and will assume that photon absorption by ices of water or CH_3NCO is negligible for longer wavelengths. The VUV absorption cross section for

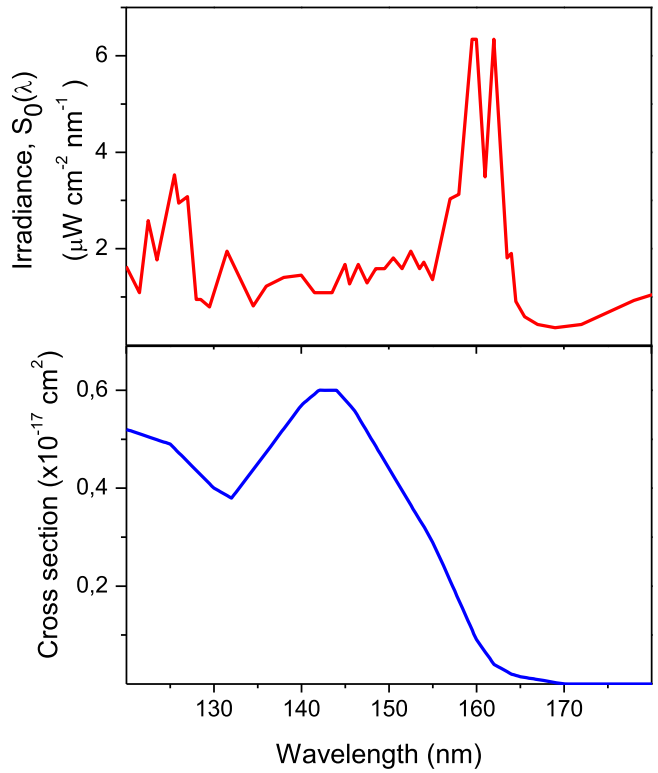

Figure 1. Upper panel: irradiance spectrum, $S_0(\lambda)$, of the UV lamp at the location of the samples (see text). Lower panel: absorption cross section of amorphous water ice at 8 K, taken from Cruz-Diaz et al. (2014).

water ice has recently been measured by Cruz-Diaz et al. (2014) and is presented in Figure 1. As far as we know, no absorption cross sections have been reported for CH_3NCO ice, but the gas-phase measurements of Tokue et al. (1987) show that UV absorption for wavelengths >180 nm is very small compared with that in the range 120–180 nm.

The irradiance profile of the lamp was provided by the manufacturer and is presented in Figure 1 at the location of the substrate (3 cm from the lamp). The integrated irradiance reaching the sample, S_0, is given by

$$S_0 = \int S_0(\lambda) d\lambda \quad (3)$$

where $S_o(\lambda)$ is the wavelength-dependent irradiance. Integrating Equation (3) over the range 120–180 nm yields $S_0 = 100\ \mu$W cm^{-2}. The corresponding photon flux, ϕ_{ph}, is derived as

$$\phi_{ph} = \int \phi_{ph}(\lambda) d\lambda = \int S_0(\lambda) \frac{\lambda}{hc}\, d\lambda \quad (4)$$

where h is Planck's constant and c the speed of light. Integration of Equation (4) over the interval 120–180 nm leads to $\phi_{ph} = 7.5 \times 10^{13}$ photons cm^{-2} s^{-1}.

For the electron bombardment experiments, we used 5 keV electrons from an electron gun built in our laboratory (Maté et al. 2014). The gun provides a homogeneous electron flux covering the whole area of the exposed Si substrate (a circle of diameter 1 cm) available for deposition and IR spectroscopy. As in previous works (Maté et al. 2015, 2016), care was taken to ensure that the electron penetration depth was larger than the thickness of the ice samples. The flux at the substrate was measured to be $\phi_e = 4 \times 10^{12}$ electrons cm^{-2} s^{-1}. The relevant sample properties and processing conditions are summarized in Table 1.

IR spectra of the ices were recorded as a function of processing time, and special attention was paid to the decay of the asymmetric stretching band, ν_a–NCO, of CH_3NCO. In our experiments, vapor deposition from the background gas takes place simultaneously on both sides of the substrate, whereas UV irradiation and electron bombardment are performed on just one side. In order to correct for the effect of the unprocessed face of the substrate, the IR spectrum of the freshly deposited samples was divided by two and subtracted from the spectra taken in the course of energetic processing. With a base pressure of $\sim(0.7–1) \times 10^{-8}$ mbar, water vapor from the chamber deposited on our samples at an approximate rate of $\sim(3–6) \times 10^{15}$ molecules cm^{-2} hr^{-1}. The effect was small in the electron bombardment experiments, which lasted for less than an hour. In the longer (about 5 hr), UV irradiation experiments the deposited water was well within the estimated uncertainty of the H_2O column density of the mixed $CH_3NCO(4\%)/H_2O$ ice, but it had some influence on the spectrum of pure CH_3NCO ice, especially in the OH stretching region around $\sim$3200 cm^{-1}. The effect was corrected by subtracting the appropriate H_2O spectrum from the spectra of the irradiated samples. Finally, to check the effect of temperature on methyl isocyanate diluted in water, ice samples of $CH_3NCO(4\%)/H_2O$ mixtures were heated from deposition temperature (20 K) until sublimation at a rate of 5 K minute^{-1}. To record the IR spectra, heating was halted at the selected temperatures.

3. Results and Discussion

3.1. Main Processing Products

The effects of UV irradiation and electron bombardment on the samples of pure CH_3NCO ice and of CH_3NCO diluted in water ice are reflected in the IR spectra of Figures 2–5. In the unprocessed samples the ν_a–NCO band, with its characteristic quadruplet structure, stands out at 2400–2200 cm^{-1}. There are some differences in the peak positions and in the band profiles between the spectra of pure methyl isocyanate and those of methyl isocyanate diluted in water ice, but the characteristic quadruplet structure is present in both cases (see Maté et al. 2017 for a discussion on the IR spectroscopy). The ν_a–NCO band is the most intense IR absorption of methyl isocyanate. After sufficiently long processing, this band virtually disappears and is replaced by four new bands, which are assigned to stretching vibrations of CO_2, OCN^-, CO, and HCN or CN^- (see upper panels of Figures 3 and 5). The locations of the new band maxima for the different samples are listed in Table 2. Note that the same products are obtained in all cases although their relative abundances are very different. In the ices of pure methyl isocyanate (Figures 2 and 3), the main product bands are those of CO_2 and CO, which appear with comparable intensities. In contrast, in the ices of CH_3NCO diluted in H_2O (Figures 4 and 5), the spectra of the products are largely dominated by the CO_2 band. In the mixture processed with electrons (S4) the HCN/CN^- feature is hardly visible. The peak frequencies of the neutral molecules CO_2 and CO are stable within 2 cm^{-1} for all the samples, whereas those involving the OCN^- and CN^- anions appear redshifted (between 6 and 15 cm^{-1}) in the mixtures with water ice as

Table 1
Column Densities in the Ice Samples Together with Energies and Fluxes of the Photons and Electrons used for Processing

Sample	$N(CH_3NCO)$ (molecules cm^{-2})	$N(H_2O)$ (molecules cm^{-2})	Processing Agent	φ (cm^{-2} s^{-1})
S1: CH_3NCO	$(4.5 \pm 0.9) \times 10^{16}$	...	UV (10.3–6.9 eV)	7.5×10^{13}
S2: $CH_3NCO(4\%)/H_2O$	$(2.5 \pm 0.5) \times 10^{16}$	$(6.4 \pm 0.6) \times 10^{17}$	UV (10.3–6.9 eV)	7.5×10^{13}
S3: CH_3NCO	$(4.3 \pm 0.9) \times 10^{16}$	...	Electrons, 5 keV	4×10^{12}
S4: $CH_3NCO(5\%)/H_2O$	$(3.5 \pm 0.7) \times 10^{16}$	$(6.5 \pm 0.6) \times 10^{17}$	Electrons, 5 keV	4×10^{12}

Note. The column densities correspond to the deposits formed on one side of the Si substrate.

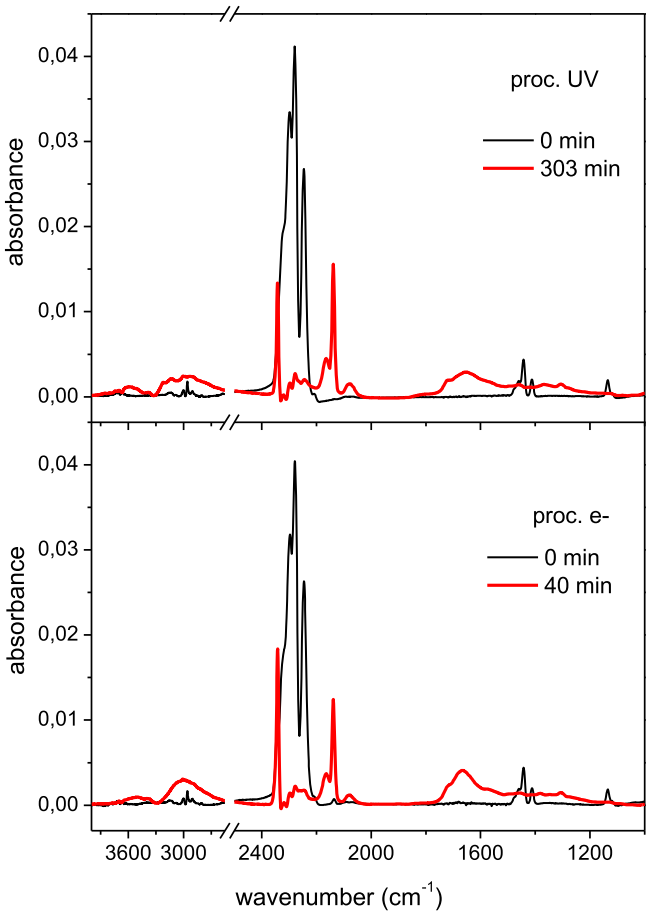

Figure 2. Effects of energetic processing on samples of pure CH_3NCO (see Table 1). Upper panel: UV irradiation of sample S1. Lower panel: electron bombardment of sample S3.

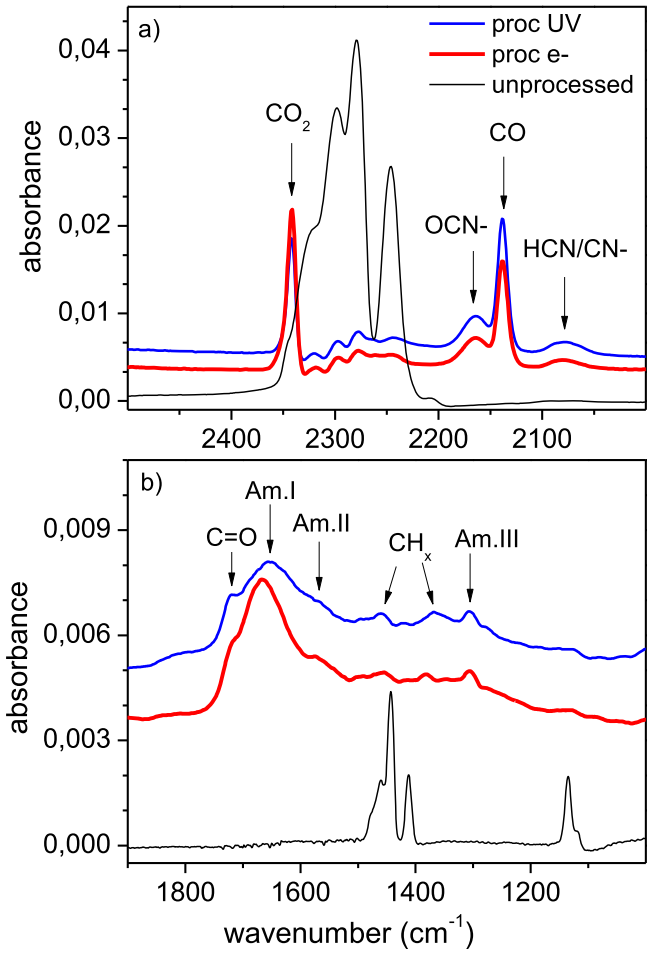

Figure 3. Detail of IR spectra of Figure 2. Am.I, Am.II, and Am.III refer to amide bands (see text and Table 2).

compared with those without water, which suggests that the CN bond is somewhat weakened in the solvated anions.

Besides the features just commented on, the spectra of processed ices of pure CH_3NCO (Figures 2 and 3) show broad absorptions, attributable to polyamides. These broad bands appear at ~3700–3300 cm^{-1} (NH stretch vibrations), ~3250–2460 cm^{-1} (stretch vibrations of CH_x alkyl groups), and 1820–1050 cm^{-1} (amide bands). The maxima of these absorptions and the peak substructure observed in the amide band region are listed and tentatively assigned in Table 2. Similar IR spectra, with peaks of CO_2, OCN^-, CO, HCN/CN^-, and amide bands, were found after the electron bombardment of pure glycine ices (Maté et al. 2015). In the processed ices of CH_3NCO diluted in H_2O, minor peaks, consistent with vibrations of CH_x groups, appear at ~2950, 1500, and 1380 cm^{-1} and a peak possibly due to a stretching of the formate anion, HCO_2^-, is found at ~1350 cm^{-1} (see Table 2). The intense water absorptions at ~4000–3000 cm^{-1} and ~1660 cm^{-1} can mask the presence of small peaks of other functional groups.

The mechanisms underlying the observed chemical transformations are not known in detail, but the similarity between the products of electron and photon processing is worth noting. In the following, we elaborate on likely reaction pathways induced by the energetic processing of the ices. Our experiments do not provide detailed mechanistic information, and the discussion, based on the observed final spectra and on literature sources, remains to a large extent speculative.

Two primary dissociation channels were identified in the gas-phase photolysis of CH_3NCO with UV photons of 210 nm

Table 2
IR Bands of the Products of CH_3NCO Ice Processing

IR Frequencies of the Products of Ice Processing (cm^{-1})				Assignment
S1	S2	S3	S4	
CH_3NCO, UV	$CH_3NCO(4\%)/H_2O$, UV	CH_3NCO, electrons	$CH_3NCO(5\%)/H_2O$, electrons	
3572 (3700–3300)		3524 (3701–3302)		ν–NH
2951 (3285–2466)		3006 (3247–2466)		ν–CH_x
	2920–2800		2920–2800	ν–CH_x
2342	2342	2342	2342	CO_2, ν_a
2165	2172	2165	2171	OCN^-, ν–CN
2138	2137	2139	2137	CO, ν
2075	2091	2078	2092	HCN/CN^-, ν–CN
1814–1055		1823–1054		Amide bands
1728		1716		ν–C=O
1651		1667		Amide I (mostly ν–C=O)
1570		1570		Amide II (mostly in-phase δ–NH + ν–CN)
	1499		1498	H_2CO, δ–CH_2
1460		1455		δ–CH_x
1363	1380	1378	1378	δ_s–CH_x
	1352		1351	HCO_2^-, ν_s–CO
1303		1301		Amide III (mostly out-of-phase δ–NH + ν–CN)

Note. For the band assignment see Boogert et al. (2015), Hudson et al. (2001), Moore & Hudson (2003), Hudson & Moore (2004), Gálvez et al. (2010), Maté et al. (2012a, 2016), Cannon (1960), Barth & Zscherp (2002). Symbols ν and δ stand for stretch and deformation vibrations respectively.

(Bamford & Bamford 1941):

$$CH_3NCO + UV \rightarrow CH_3N + CO \quad (5)$$

$$CH_3NCO + UV \rightarrow CH_3 + NCO. \quad (6)$$

The same dissociation pathways can be assumed to hold for solid-state CH_3NCO. The radicals produced in the photolysis are highly reactive and can start a chain of reactions in the ice leading to stable molecular species or even polymers. With increasing photon energy, additional channels become open. The radical CH_2NCO, for instance, which corresponds to the breaking of a CH bond, was identified in the radiolysis of frozen CH_3NCO at 77 K with ^{60}Co γ-rays (Symons & Trousson 1984). The formation of OCN^- was observed by Hudson et al. (2001) after bombarding mixtures of C_2H_5NCO and H_2O at 16 K with 0.8 MeV protons. The protons induce a cascade of secondary electrons in the ice and the authors of that work suggested that OCN^- is formed through dissociative electron attachment to C_2H_5NCO. The OCN^- anion, a linear molecule with 16 valence electrons like CO_2, is a stable species, especially at cryogenic temperatures. A similar mechanism can be assumed for the electron bombardment of methyl isocyanate ice in the present work:

$$CH_3NCO + e \rightarrow CH_3 + OCN^-. \quad (7)$$

The location of the negative charge on the OCN fragment is the obvious outcome of the dissociative attachment because OCN has a high electron affinity (3.61 eV, as measured by Bradforth et al. 1993) and the CH_3^- anion is less stable than the methyl radical (Marynick & Dixon 1977). The fact that a similar OCN^- proportion is found in the UV photolysis and electron bombardment experiments (Figures 2 and 3) may be puzzling at first sight, since the photon energy of the present experiments (<10.3 eV) is small compared with the ionization potentials of the molecules present in the ices. However, the threshold for photoionization of molecules in polar ices might be appreciably lower than that of the same molecules in the gas phase, as discussed in Gerakines et al. (2000) and Woon (2004). This would make electrons and ions available for chemistry in the UV-irradiated ices. Chemical processes involving the dissociation products of reactions (5) and (6) can also contribute to the formation of the secondary products CO_2 and HCN, and possibly also the anions OCN^- and CN^-. Low-temperature acid–base chemistry is often invoked to explain the appearance of charged species in ices (Hudson et al. 2001; Raunier et al. 2004; Gálvez et al. 2010; Theulé et al. 2013) and it might also be relevant for the formation of the anions in our experiments, but in the case of the pure CH_3NCO samples the reaction pathways are not obvious. The formation of aggregates and polymers in the processing of pure CH_3NCO ices is not entirely surprising. The polymerization of isocyanates in the liquid phase at low temperatures to yield polyamides was described in the sixties by Shashoua et al. (1960). These authors suggest a polymerization mechanism based on anionic catalysis. A similar mechanism could be at play in the present ice processing experiments.

In the irradiation of diluted mixtures of CH_3NCO in water ice (Figures 4 and 5), additional destruction mechanisms are possible. Hydrolysis of methyl isocyanate is known to produce CO_2 in a two-step process (Castro et al. 1985):

$$CH_3NCO + H_2O \rightarrow CH_3NHCO_2H, \quad (8a)$$

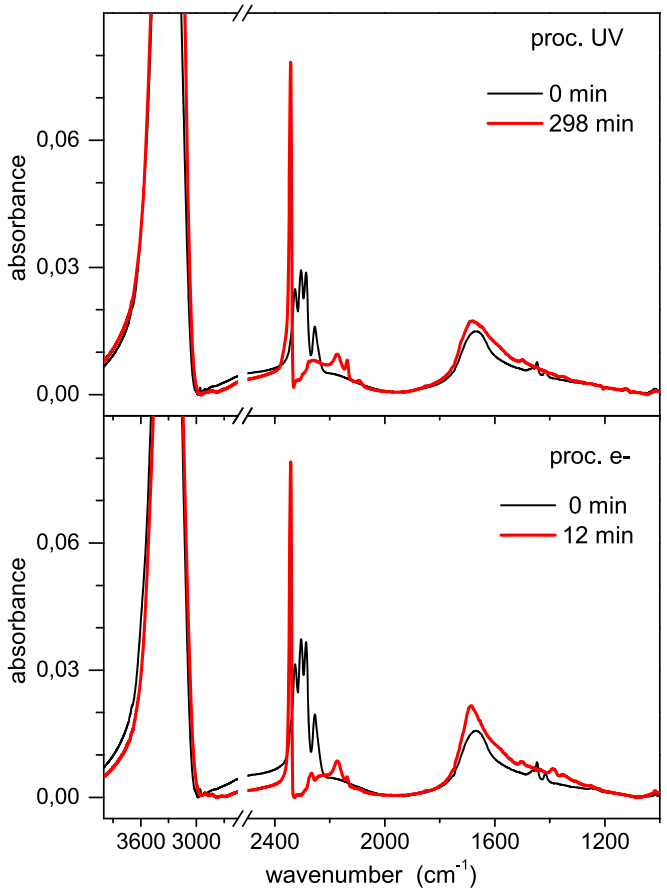

Figure 4. Effects of energetic processing on samples of CH_3NCO diluted in water ice (see Table 1). Upper panel: UV irradiation of sample S2 (4% CH_3NCO in H_2O). Lower panel: electron bombardment of sample S4 (5% CH_3NCO in H_2O).

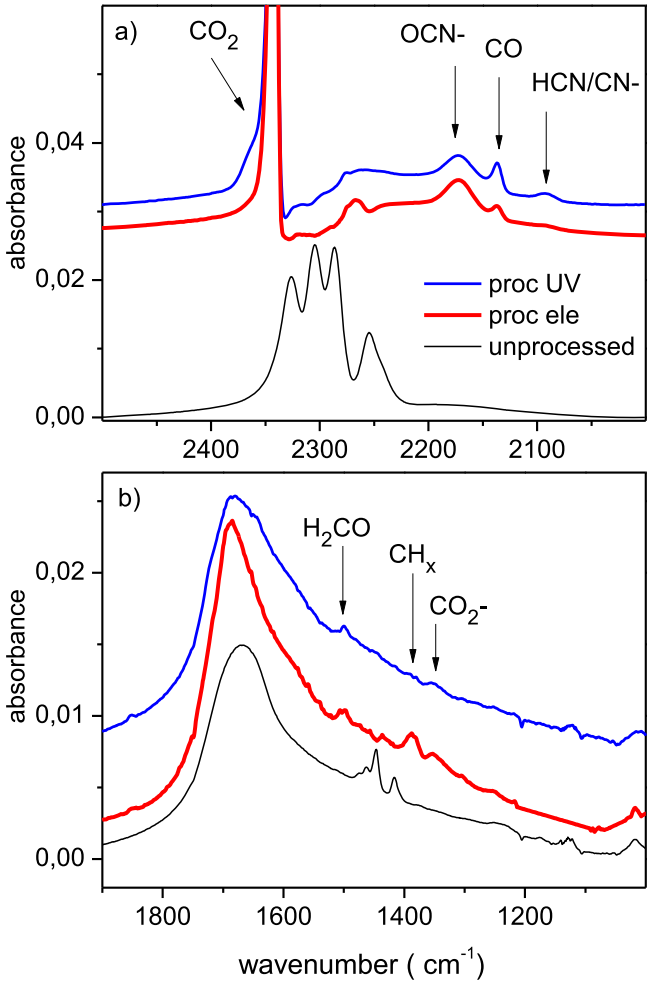

Figure 5. Detail of IR spectra of Figure 4 (see text and Table 2).

$$CH_3NHCO_2^- + H^+ \rightarrow CH_3NH_2 + CO_2. \quad (8b)$$

This reaction does not take place at the low temperatures of the experiments (see Section 3.3) but it could be activated if either H_2O or CH_3NCO is internally excited during irradiation. In the mixed ices, the dissociation of water plays a key role in the chemistry. The photolysis and radiolysis of water ice have been extensively studied by many groups (see Johnson & Quickenden 1997 and references therein). Photolysis takes place for UV photons with $\lambda < 280$ nm and the main dissociation channel is

$$H_2O + UV \rightarrow OH + H. \quad (9)$$

Subsequent photolysis of OH can lead to the production of O and H. Charged species can also be formed especially in the bombardment with highly energetic ions or electrons. The primary dissociation products, H and OH, recombine easily to H_2O, but some of the atoms and ions react further, and in pure water ice this lead to the formation of small amounts of HO_2, H_2O_2, O_2, and H_2. In the mixtures, H atoms and OH radicals can also react with CH_3NCO. In the recent work of Belloche et al. (2017) hydrogenation of CH_3NCO with H atoms has been suggested as a possible mechanism for formation of N-methylformamide (CH_3NHCOH) in dense clouds. We are not aware of published spectra of CH_3NHCOH ices but recent measurements in cold Ar matrices (Sałdyka et al. 2014) reveal the presence of two peaks at 1725 cm^{-1} (ν–CO) and 1518 cm^{-1} (δ–NH + ν–CN) that are not seen in our experiments; nevertheless the presence of N-methylformamide cannot be totally ruled out since the most intense of these peaks (ν–CO at 1725 cm^{-1}) might be blended with the intense bending mode of water at ~1660 cm^{-1}. In fact, the shape of the 1660 cm^{-1} band changes upon processing and its maximum shifts towards 1700 cm^{-1}.

OH radicals destroy CH_3NCO molecules in the gas phase (Lu et al. 2014) and presumably in the solid phase too. In the ices, the hydroxyl radical is also known to react swiftly with CO (Oba et al. 2010):

$$CO + OH \rightarrow CO_2 + H. \quad (10)$$

Reaction (10) is thought to be the main mechanism leading to the transformation of CO into CO_2 in the photolysis (Allamandola et al. 1988; Watanabe & Kouchi 2002) and radiolysis (Hudson & Moore 1999) of diluted CO/H_2O mixtures at low T. In the present work, most of the CO appearing as a primary dissociation product of CH_3NCO in reaction (5) would be immediately transformed to CO_2 through reaction (10), and that would contribute to the preponderance of the CO_2 band in the IR spectra of the products (see Figure 4 and upper panel of Figure 5). The reaction of H atoms with CO could lead to the formation of formaldehyde and methanol (see

Fuchs et al. 2009; Hama & Watanabe 2013 and references therein), and in fact a small peak at ~1500 cm^{-1}, attributable to H_2CO, appeared in the spectra of processed CH_3NCO/H_2O samples. The ν–CO vibration of the molecule at ~1720 cm^{-1} was not seen, but as indicated above it could be blended with large bending absorption of water at 1660 cm^{-1}. Other chemical reactions, and particularly low-temperature acid–base chemistry, may be favored in water ice where species like H^+ and OH^- can be formed; but, in any case, under our experimental conditions, the breakdown of CH_3NCO into smaller fragments prevails over any chemistry leading to complex molecules.

3.2. Destruction Cross Sections and Half-life Doses

The destruction rate of CH_3NCO during irradiation with photons or electrons can be followed by monitoring the decay of the ν_a–NCO band. Assuming a first-order irreversible process, the decrease of the band intensity can be expressed as

$$\ln\left(\frac{I_F}{I_0}\right) = -\sigma F \tag{11}$$

where F is the fluence (photons or electrons cm^{-2}), I_F the band intensity (absorbance) for a given fluence, I_0 the band intensity before irradiation, and σ an effective destruction cross section. In the case of UV photolysis, both the cross section and the fluence depend on the photon wavelength, but our experiment yields only a cross section corresponding to the fluence integrated over the relevant wavelength range (120–180 nm). The experimental values of $\ln(I_F/I_0)$ are presented in Figure 6 as a function of F, and destruction cross sections can be obtained from a fit of these data to Equation (11). The experimental details and cross-section values for the four samples studied are given in Table 3. The integrated half-life fluence, i.e., the fluence needed to decrease the initial CH_3NCO concentration by one half, is readily derived from Equation (11) as

$$F_{1/2} = \ln(2)/\sigma. \tag{12}$$

A useful measure of the destruction efficiency is the half-life dose. In the UV processing experiments it can be calculated as

$$D_{1/2} = \frac{1}{N_{CH_3NCO}} \int F_{1/2}(\lambda) E(\lambda) f_E(\lambda) d\lambda \tag{13}$$

where N_{CH_3NCO} is the column density of methyl isocyanate, and $F_{1/2}(\lambda)$, $E(\lambda)$, and $f_E(\lambda)$ are, respectively, the half-life fluence, the photon energy, hc/λ, and the fraction of the incident energy absorbed by the sample for a given wavelength. The product $F_{1/2}(\lambda)E(\lambda)$ can be expressed in terms of the incident irradiance as

$$F_{1/2}(\lambda)E(\lambda) = S_0(\lambda) F_{1/2} \phi_{ph}^{-1} \tag{14}$$

where $F_{1/2}$ is the integrated half-life fluence given by Equation (12) and ϕ_{ph} the integrated photon flux (note that the product $F_{1/2}\varphi_{ph}^{-1}$ is the half-life time, $t_{1/2}$). Substituting in Equation (13), we have

$$D_{1/2} = \frac{\ln(2)}{\sigma \phi_{ph} N_{CH_3NCO}} \int S_0(\lambda) f_E(\lambda) d\lambda. \tag{15}$$

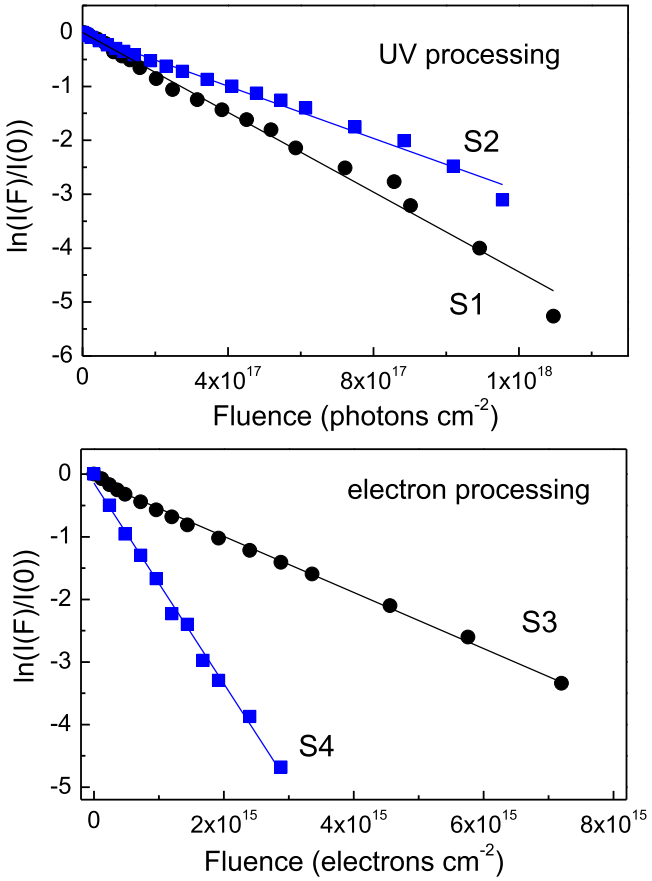

Figure 6. Decay of the intensity of the ν_a–NCO band (2372–2194 cm^{-1}) during UV irradiation (upper panel) and electron bombardment (lower panel) at 20 K. The labels S1–S4 correspond to the samples of Table 1. In the UV irradiation experiments the fluence corresponds to the photon flux integrated over the interval 120–180 nm (see text). Note the different scale ranges of the horizontal axis. Black circles: samples of pure CH_3NCO ice. Blue squares: samples of CH_3NCO diluted in water ice. The lines correspond to a fit of the data to Equation (11). The experimental details and fitted cross-section values are listed in Tables 1 and 3.

The fraction of energy absorbed can be expressed as

$$f_E(\lambda) = 1 - \frac{S(\lambda)}{S_0(\lambda)} \tag{16}$$

where $S(\lambda)$ is the irradiance transmitted through the sample, which can be calculated using Beer's law. In the UV irradiation of CH_3NCO diluted in water ice (sample S2), the energy is absorbed essentially by the much more abundant H_2O molecules and we have neglected the absorption by CH_3NCO. With this assumption Equation (15) can be written as

$$D_{1/2} = \frac{\ln(2)}{\sigma \phi_{ph} N_{CH_3NCO}} \int S_0(\lambda)(1 - e^{-\sigma_{H2O}(\lambda) N_{H2O}}) d\lambda \tag{17}$$

where $\sigma_{H2O}(\lambda)$ and N_{H2O} are the absorption cross section and the column density of H_2O. The CH_3NCO destruction cross section, σ, for sample S2 is also listed in Table 3. The column densities N_{CH_3NCO}, N_{H2O} and the integrated photon flux, φ_{ph}, are taken from Table 1. $S_0(\lambda)$ and $\sigma_{H2O}(\lambda)$ are displayed in Figure 1. The half-life dose, derived by integrating Equation (17) over the range 120–180 nm, is given in Table 3.

Table 3
Photolysis and Radiolysis of CH_3NCO in the Ices of this Study

Sample	Processing Agent	Destruction Cross Section, σ (cm^{-2})	Fraction of Energy Absorbed	Half-life Doses, $D_{1/2}$ (eV $molecule^{-1}$)
S1: CH_3NCO	UV (10.3–6.9 eV)	$(3.7 \pm 0.1) \times 10^{-18}$	0.15 ± 0.03	5 ± 2
S2: $CH_3NCO(4\%)/H_2O$	UV (10.3–6.9 eV)	$(2.4 \pm 0.05) \times 10^{-18}$	0.68 ± 0.14	64 ± 19
S3: CH_3NCO	Electrons, 5 keV	$(4.5 \pm 0.1) \times 10^{-16}$	0.05 ± 0.007	9 ± 2
S4: $CH_3NCO(5\%)/H_2O$	Electrons, 5 keV	$(1.6 \pm 0.04) \times 10^{-15}$	0.30 ± 0.04	18 ± 5

For the pure CH_3NCO sample (S1) we have assumed that the irradiation of the sample leads essentially to the destruction of the molecules and we have approximated the absorption cross section to the destruction cross section. In this case the λ dependence of the cross section is unknown and we can only use the averaged value given in Table 3. Equation (17) transforms into

$$D_{1/2} = \frac{\ln(2)}{\sigma \phi_{\rm ph} N_{\rm CH_3NCO}} (1 - e^{-\sigma N_{\rm CH_3NCO}}) \int S_0(\lambda) d\lambda. \quad (18)$$

The corresponding half-life dose is also listed in Table 3.

In the electron bombardment experiments (samples S3 and S4), Equation (13) reduces to

$$D_{1/2} = \frac{F_{1/2} E f_E}{N_{\rm CH_3NCO}} \quad (19)$$

where $F_{1/2}$ is obtained from Equation (12) with the cross sections of Table 3, and values of $N_{\rm CH_3NCO}$ and E are taken from Table 1. The fraction of energy, $f_{\rm E}$, deposited into the ices by the impinging electrons was calculated using the Monte Carlo Simulations of Electron Trajectories in Solids code (CASINO) (Drouin et al. 2007; Drouin 2011). We used CASINO version v3.2 in the Monsel CASINO physics mode. The simulations were run with 1000 electrons of 5 keV and trajectories were stopped for electron energies <50 eV. Input parameters also include densities and thicknesses of the processed samples. We derived the thickness values from the column densities of Table 1. A density of 1 g cm^{-3} was assumed for the pure CH_3NCO ice (sample S3). The corresponding sample thickness was 40 nm. For the sample of CH_3NCO diluted in water (sample S4) we considered just the absorption by the much more abundant water molecules. A thickness of 300 nm was obtained for this sample assuming a water density of 0.64 g cm^{-3}, which corresponds to porous amorphous water, vapor-deposited at 20 K (Maté et al. 2012b). The half-life doses for the electron bombardment experiments are listed in Table 3.

The highest destruction efficiency is achieved, as expected, for the pure CH_3NCO samples. Only a small fraction of the photons and electrons are absorbed by these thin deposits, but all the energy absorbed is invested in the dissociation of methyl isocyanate. The high half-life dose obtained for the UV photolysis of CH_3NCO diluted in water ice is worth noting. The energy of the irradiating photons (<10.3 eV) is enough to dissociate the molecule, and even to produce some ionization, but the excess energy carried by the H and OH fragments is relatively small and they do not travel far within the ice. Their most likely fate is recombination to H_2O, a process enhanced by the "cage effect" of the solid environment. In this case, the CH_3NCO molecules are effectively shielded from the UV radiation by the water ice matrix. In contrast, the bombardment of the ice mixtures with 5 keV electrons induces a cascade of secondary electrons that propagate over comparatively long distances, provoking an extensive ionization and fragmentation of the molecules in the ice. Both the secondary electrons and the ions and radicals appearing in their wake contribute efficiently to the destruction of CH_3NCO. The differences between UV and electron processing are made apparent in Figure 6. Dilution in water ice makes the decay of CH_3NCO slower for UV irradiation, but faster for electron bombardment; as a result, the half-life dose for 5 keV electrons in the mixed ices is about 3.5 times lower than that for UV photons.

3.3. Thermal Processing

Thermal processing of ices can induce chemical reactions even at very low temperatures (see Theulé et al. 2013 and references therein) and could be largely responsible for the wealth of chemical species observed in hot cores and hot corinos (Boogert et al. 2015). In water-dominated astrophysical ices, hydrolysis is a likely reaction. Hydrolysis of CH_3NCO (Equations (8a) and (8b) above) does not take place in ice mixtures at 20 K (Maté et al. 2017) but could happen in principle for higher ice temperatures. The effects of thermal processing on the ν_a–NCO band of CH_3NCO diluted in water ice are shown in Figure 7. The measurements were carried out for an ice sample containing 4% CH_3NCO molecules. Upon heating, the band profile is modified, but no new bands appear and the overall band intensity does not change much in the temperature interval 20–150 K. As discussed elsewhere (Reva et al. 2010; Maté et al. 2017), the multiplet structure of this band is most likely due to a coupling of NCO stretching and CH_3 torsional modes. The spacing between the first torsional levels is of the order of 25–30 cm^{-1} and their populations should undergo significant variations with growing ice temperature, which would explain the observed modification of the band profile.

Between 150 and 160 K, the process of "volcano desorption" (Smith et al. 1997) of CH_3NCO associated with ice crystallization expels CH_3NCO from the solid and leads to a marked decrease in the band intensity. Finally, the band disappears with ice sublimation. The absence of new peaks, and specifically of the 2345 cm^{-1} peak of CO_2, indicates that methyl isocyanate is stable against hydrolysis over the temperature range of relevance for astronomical ices.

4. Astrophysical Implications

We can use the experimental results of this study to estimate the survival probability of methyl isocyanate in Kuiper Belt Objects (KBOs) and in the icy mantles of dust grains in cold clouds, where molecules are subjected to UV fields and CR bombardment. The Kuiper Belt, at a distance of ~30–50 au from the Sun, is a major comet reservoir and was the original location of comet 67P/CG (Dones et al. 2015). Although ices in space are a mixture of various species (H_2O, CO_2, CO) we

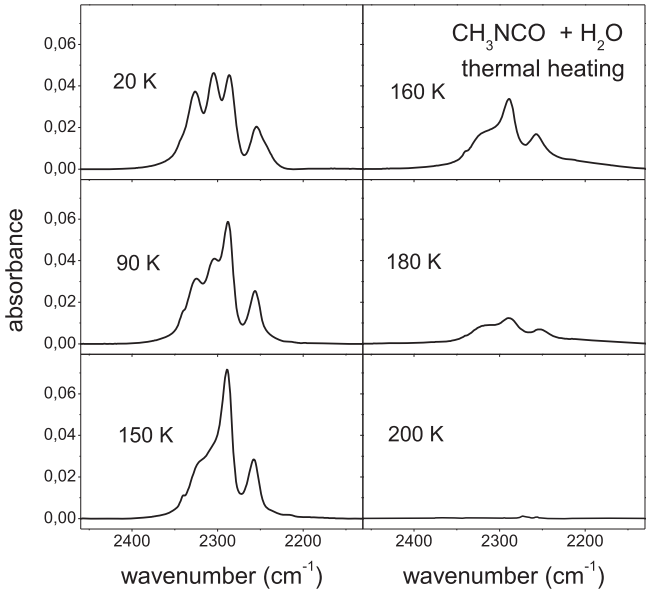

Figure 7. Evolution of the ν_a–NCO band of CH_3NCO during the heating of a CH_3NCO (4%)/H_2O ice mixture.

assume that the results obtained for CH_3NCO molecules diluted in water ice studied in this work are representative of the behavior of hypothetical CH_3NCO molecules in astronomical ices, since H_2O is always the dominant component. As mentioned above, we also assume that high-energy electrons simulate the effects of CRs.

The half-lives estimated for CH_3NCO molecules in KBOs or dense clouds subjected to either UV irradiation or CR bombardment are listed in Table 4. For these estimates we have used the half-life doses of Table 3 for CH_3NCO molecules diluted in water ice (samples S2 and S4), and literature values for the corresponding UV and CR dose rates, which are also included in the table. These literature values, based on different measurements and models, contain many approximations and allow only order-of-magnitude estimates.

Comet 67P/CG is a Jupiter-family comet (JFC) with origin in the Kuiper Belt (Dones et al. 2015). The most likely physical lifetime of a JFC is of the order of $\sim 10^4$ yr (Levison & Duncan 1997), and hence the nuclei of present-day JFCs have resided mostly ($\sim 4.6 \times 10^9$ yr) in the Kuiper Belt. The fluxes of UV photons and CR particles impinging on KBOs contain a large number of comparatively slow protons from the solar wind (Cooper et al. 2003). According to the estimate of the present work, at the uppermost surface of a KBO any primeval CH_3NCO would have disappeared in just thousands of years. Furthermore, very efficient formation processes would be needed to counter the intense UV and CR bombardment and keep an appreciable surface concentration of the molecule. However, the water molecules in the ice provide a very efficient shield. Just 10 μm below the surface the UV field has disappeared and the CR flux decreases drastically due to the small penetration depth of the abundant low-energy solar protons. The estimated half-life of CH_3NCO at this depth is $\sim 10^9$ yr, of the order of the lifetime of the solar system. According to this estimate, KBOs could retain inside the ice a part of the hypothetical CH_3NCO generated in the dense cloud phase. After leaving the Kuiper Belt, the fate of molecules is more difficult to estimate, but the efficient protection provided by water ice suggests that part of the primeval CH_3NCO buried beneath the surface might survive the intense solar irradiation during the short JFC phase. When the comet approaches the Sun, dramatic changes can happen. In its present orbit, for instance, it is estimated that 67P/CG loses several centimeters of ice per year (Bieler et al. 2015). This should lead to the exposure and destruction of CH_3NCO in the outer ice layers. However, if CH_3NCO were uniformly distributed within the ice of the original comet, some of it could survive as long as there remained some ice with a thickness of the order of tens of microns.

The chemical composition of comet 67P/CG was studied by mass spectrometry in the course of the *Rosetta* mission. Mass spectra were acquired from three sources. The Ptolemy (Wright et al. 2015) and COSAC (Goesmann et al. 2015) instruments on board the Philae lander performed measurements after the first touchdown of the lander on the comet in 2014 November. COSAC sampled evaporated molecules from excavated material that entered the warm exhaust tubes located at the bottom of the lander, whereas Ptolemy sampled ambient coma gases. In 2016 September, the high-resolution DMFS spectrometer of the ROSINA experiment (Altwegg et al. 2017) also sampled molecules in the coma of the comet. Methyl isocyanate was only reported in the analysis of the COSAC data. A reanalysis of the first measurements in conjunction with the new high-resolution data from ROSINA (Altwegg et al. 2017) has shown that, due to limited mass resolution and low counting statistics, a unique interpretation of the Ptolemy and COSAC measurements is not possible. Specifically, the identification of methyl isocyanate could not be confirmed. Although the results of our experiments suggest that CH_3NCO could persist under the surface of comet 67P/CG, the work of Altwegg et al. (2017) shows that, if present at all, its abundance should be much lower than that published in the initial COSAC report (Goesmann et al. 2015).

The interior of dense clouds is shielded from the Galactic UV field by gas molecules and dust grains, but CRs reaching these regions dissociate H_2 molecules and excite H and H_2, giving rise to a secondary UV field (Prasad & Tarafdar 1983). Both CRs and secondary UV photons can destroy molecules in ice mantles. Using the estimated dose rates reported by Moore et al. (2001) for ice mantles in a dense cloud, we obtain a half-life of $\sim 1.6 \times 10^8$ yr for CH_3NCO molecules subjected to UV radiation. This time is appreciably longer than the life of a typical dense cloud ($\sim 10^7$ yr) and reflects the effective UV shielding provided by water ice already commented on in Section 3.2. The half-life of CH_3NCO against CRs is $\sim 6 \times 10^7$ yr, still longer than the cloud's lifetime. Consequently, although a fraction of the hypothetical CH_3NCO would be destroyed, mainly by CRs, in the dense cloud, some of it could survive the cloud collapse. As shown in Section 3.3, the molecule is stable in ice until sublimation and would desorb to the gas phase in hot cores, where it has been observed. In particular, in Orion KL, more than 400 rotational lines of CH_3NCO were identified by Cernicharo et al. (2016).

5. Summary and Conclusions

The stability of methyl isocyanate ices against UV radiation and CRs has been investigated in the laboratory. Ices of pure CH_3NCO and of CH_3NCO(4%–5%)/H_2O mixtures were deposited from the vapor phase on a substrate held at 20 K.

Table 4
Estimated CH_3NCO Half-life in Dense Clouds and Cometary Ices

Location of Ices in Space	Lifetime of Ices (yr)	Depth (cm)	UV Dose Rate (eV molecule^{-1} yr^{-1})	UV CH_3NCO Half-life (yr)	CR Dose Rate (eV molecule^{-1} yr^{-1})	CR CH_3NCO Half-life (yr)
Kuiper Belt Object	4.6×10^9	...	2.2×10^{-2}[a]	1.1×10^4	5.6×10^{-3} [b]	3.2×10^3
(40 au)		10^{-3}	...	...	1.6×10^{-8} [c]	1.1×10^9
Cold dense cloud	10^7	...	4×10^{-7}[d]	1.6×10^8	3×10^{-7} [d]	6×10^7

Notes. The half-life doses for CH_3NCO diluted in H_2O (samples S2 and S4) were used for these estimates. Literature dose rates refer to absorption by the dominant H_2O (18 amu) ice molecules.
[a] Moore & Hudson (2005). UV dose rates are estimated for the top 1.5×10^{-6} cm of the ice.
[b] Cooper et al. (2003). CR dose rate for ice thickness $<1 \times 10^{-6}$ cm.
[c] Strazzulla et al. (2003).
[d] Moore et al. (2001). UV dose rates are estimated for typical grain mantles with a thickness of 2×10^{-6} cm.

The ices were then irradiated with a deuterium lamp, emitting in the range 120–400 nm, and bombarded with high-energy (5 keV) electrons, which are assumed to mimic CRs. The destruction of the molecule in the course of energetic processing is followed by monitoring the decay of the ν_a–NCO IR band ($\sim$2372–2200 cm^{-1}). The main results of the study are the following.

1. Energetic processing of CH_3NCO ices for a sufficiently long time leads to the total destruction of the parent molecule and to the appearance of IR bands corresponding to CO, CO_2, OCN^-, and HCN/CN^-. The formation of polyamides has also been observed. The results are very similar for photon and electron processing. In samples of pure CH_3NCO the major products are CO_2 and CO, which are present in comparable amounts. In the mixed $CH_3NCO(4\%–5\%)/H_2O$ ices, the dominant product by far is CO_2. Minor peaks in the IR spectra point to the formation of small amounts of other molecules, among them possibly H_2CO, formate ions, and species containing alkyl (CH_x) groups.
2. Destruction cross sections can be derived from the decay of the CH_3NCO concentration, which is well described by a first-order irreversible reaction for both photons and electrons. The faster decay observed in the electron bombardment of mixed ices indicates that dissociation products from H_2O contribute effectively to the destruction of methyl isocyanate.
3. Water ice provides an effective shield for CH_3NCO against UV irradiation, as reflected by the high half-life energy dose ($\sim$64 eV $molecule^{-1}$) obtained for the $CH_3NCO(4\%)/H_2O$ mixture. The majority of the absorbed photons dissociate water molecules into H and OH, but most fragments recombine again to H_2O before reacting with CH_3NCO.
4. CH_3NCO is stable in water ice. The molecule does not react with water over the temperature range 20–200 K.
5. Estimates based on the present measurements and on literature values of UV and CR fluxes indicate that methyl isocyanate should be stable against UV radiation and relatively stable against CRs in the mantles of dust grains over the lifetime of a typical dense cloud ($\sim10^7$ yr). An appreciable fraction of hypothetical CH_3NCO formed in the grain mantles should survive to the hot core phase. In an object in the Kuiper Belt (the original location of comet 67P/CG), CH_3NCO should be readily destroyed on the surface by both UV photons and CRs, but it would persist for $\sim10^9$ yr under 10 μm of water ice.

This work has been funded by the Spanish MINECO under grants FIS2013-48087-C2-1P, FIS2016-C3-1P, and AYA2016-75066-C2-1-P. J.-C.G. and J.C. also thank the ANR-13-BS05-0008 IMOLABS and J.-C.G. thanks the Program PCMI (INSU-CNRS) and the Centre National d'Etudes Spatiales (CNES) for funding support. European Union funding under grant ERC-2013-Syg 610256 (NANOCOSMOS) is also acknowledged.

ORCID iDs

J. C. Guillemin https://orcid.org/0000-0002-2929-057X
J. Cernicharo https://orcid.org/0000-0002-3518-2524
V. J. Herrero https://orcid.org/0000-0002-7456-4832

References

Allamandola, L. J., Sandford, S. A., & Valero, G. J. 1988, Icar, 76, 225
Altwegg, K., Balsiger, H., Berthelier, J. J., et al. 2017, MNRAS, 469, S130
Bamford, D. A., & Bamford, C. H. 1941, J. Chem. Soc. Subdivision, 1, 30
Baratta, G. A., Leto, G., & Palumbo, M. E. 2002, A&A, 384, 343
Barth, A., & Zscherp, C. 2002, Quart. Rev. Biophys., 35, 369
Belloche, A., Meshcheryakov, A. A., Garrod, R. T., et al. 2017, A&A, 601, A49
Bieler, A., Altwegg, K., Balsiger, H., et al. 2015, Natur, 526, 678
Boogert, A. C., Gerakines, P. A., & Whittet, D. C. B. 2015, ARA&A, 53, 541
Bradforth, S. E., Kim, E. H., Arnold, D. W., & Neumark, D. M. 1993, JChPh, 98, 800
Cannon, C. G. 1960, AcSpe, 16, 302
Castro, E. A., Moodie, R. B., & Sansom, P. J. 1985, in J. Chem. Soc. Perkin Transac. II (London: The Royal Society of Chemistry), 737
Cernicharo, J., Kisiel, Z., Tercero, B., et al. 2016, A&A, 587, L4
Cooper, J. F., Christian, E. R., Richardson, J. D., & Wang, C. 2003, EM&P, 92, 261
Cruz-Diaz, G. A., Muñoz Caro, G. M., Chen, Y.-J., & Yih, T. S. 2014, A&A, 562, A119
Dones, L., Brasser, M., Kaib, N., et al. 2015, SSRv, 197, 191
Drouin, D. 2011, CASINO: monte CArlo SImulation of electroN trajectory in sOlids, http://www.gel.usherbrooke.ca/casino
Drouin, D., Couture, A. R., Joly, D., et al. 2007, Scanning, 29, 92
Fuchs, G. W., Cuppen, H. M., Ioppolo, S., et al. 2009, A&A, 505, 629
Gálvez, O., Maté, B., Herrero, V. J., & Escribano, R. 2010, ApJ, 724, 539
Gálvez, O., Ortega, I. K., Maté, B., et al. 2007, A&A, 472, 691
Gerakines, P. A., Moore, M. H., & Hudson, R. L. 2000, A&A, 357, 793
Goesmann, F., Rosenbauer, H., Brederhöft, J. H., et al. 2015, Sci, 349, aab0689
Halfen, D. T., Ilyushin, V. V., & Ziurys, L. M. 2015, ApJL, 812, L5
Hama, T., & Watanabe, N. 2013, ChRv, 107, 8783
Han, D. H., Pearson, P. G., & Baillie, T. A. 1989, J. Lab. Comp. Radiopharm, 27, 1371
Hudson, R. L., & Moore, M. H. 1999, Icar, 140, 451
Hudson, R. L., & Moore, M. H. 2004, Icar, 172, 466
Hudson, R. L., Moore, M. H., & Gerakines, P. A. 2001, ApJ, 550, 1140
Jamieson, C. S., Alexander, M. M., & Kaiser, R. I. 2006, ApJS, 163, 184
Johnson, R. E., & Quickenden, T. I. 1997, JGR, 102, 10985
Kaiser, R. I., Stockton, A. M., Kim, Y. S., Jensen, E. C., & Mathies, R. A. 2013, ApJ, 765, 111
Levison, H. F., & Duncan, M. J. 1997, Icar, 127, 13
Ligterink, N. F. W., Coutens, A., Kofman, V., et al. 2017, MNRAS, 469, 2219
Linnartz, H., Bossa, J. P., Bouwman, J., et al. 2011, in IAU Symp. 280, The Molecular Universe, ed. J. Cernicharo & R. Bachiller (Cambridge: Cambridge Univ. Press), 390
Lu, Z., Hebert, V. R., & Miller, G. C. 2014, J. Agric. Food Chem., 62, 1792
Majumdar, L., Loison, J.-C., Ruaud, M., et al. 2018, MNRAS, 473, L59
Martín-Doménech, R., Rivilla, V. M., Jiménez-Serra, I., et al. 2017, MNRAS, 469, 2230
Marynick, D. S., & Dixon, D. A. 1977, PNAS, 74, 410
Mason, N. J., Binukumar, N., Jheeta, S., & Szymanska, E. 2014, FaDi, 168, 235
Mastrapa, R. M., Sandford, S. A., Roush, T. L., Cruikshank, D. P., & D'Alle Ore, C. M. 2009, ApJ, 701, 1347
Maté, B., Herrero, V. J., Rodríguez-Lazcano, Y., et al. 2012a, ApJ, 759, 90
Maté, B., Medialdea, A., Moreno, M. A., Escribano, R., & Herrero, V. J. 2003, JPhB, 107, 11098
Maté, B., Molpeceres, G., Jiménez-Redondo, M., Tanarro, I., & Herrero, V. J. 2016, ApJ, 831, 51
Maté, B., Molpeceres, G., Timón, V., et al. 2017, MNRAS, 470, 4222
Maté, B., Rodríguez-Lazcano, Y., & Herrero, V. J. 2012b, PCCP, 14, 10595
Maté, B., Tanarro, I., Escribano, R., Moreno, M. A., & Herrero, V. J. 2015, ApJ, 806, 151
Maté, B., Tanarro, I., Moreno, M. A., et al. 2014, FaDi, 168, 267
Moore, M. H., & Hudson, R. L. 2003, Icar, 161, 486
Moore, M. H., & Hudson, R. L. 2005, in IAU Symp. 231, Astrochemistry: Recent Success and Current Challenges, ed. D. C. Lis, G. S. Blake, & E. Herbst (Cambridge: Cambridge Univ. Press), 247
Moore, M. H., Hudson, R. L., & Gerakines, P. A. 2001, AcSpA, 57, 843
Oba, Y., Watanabe, N., Kouchi, A., Hama, T., & Pirronello, V. 2010, ApJL, 712, L174
Öberg, K. I. 2016, ChRv, 116, 9631
Pascal, R., Boiteau, L., & Commeyras, A. 2005, Top. Curr. Chem., 259, 69
Prasad, S. S., & Tarafdar, S. P. 1983, ApJ, 267, 603

Quénard, D., Jiménez-Serra, I., Viti, S., Holdship, J., & Coutens, A. 2018, MNRAS, 474, 2796
Raunier, S., Chiavassa, T., Marinelli, F., & Aycard, J. P. 2004, CP, 352, 259
Reva, I., Lapinski, L., & Fausto, R. 2010, JMoSt, 976, 333
Sałdyka, M., Mielke, Z., Mierzwicki, K., Coussan, S., & Roubin, P. 2014, PCCP, 13, 13992
Shashoua, V. E., Sweny, W., & Tietz, R. F. 1960, JACS, 82, 866
Smith, R. S., Huang, C., Wong, E. K. L., & Kay, B. D. 1997, PhRvL, 79, 909
Strazzulla, G., Cooper, J. F., Christian, E. R., & Johnson, R. E. 2003, CRPhy, 4, 791
Symons, M. C. R., & Trousson, P. M. 1984, RaPC, 23, 127
Tercero, B., Cernicharo, J., Pardo, J. R., & Goicoechea, J. R. 2010, A&A, 517, 96
Tercero, B., Margullès, L., Carvajal, M., et al. 2012, A&A, 538, A119
Theulé, P., Duvernay, F., Danger, G., et al. 2013, AdSpR, 52, 1567
Tokue, I., Hiraya, A., & Shobatake, K. 1987, CP, 117, 315
Watanabe, N., & Kouchi, A. 2002, ApJ, 567, 651
Woon, D. E. 2004, AdSpR, 33, 44
Wright, I. P., Sheridan, S., Barber, S. J., et al. 2015, Sci, 349, aab0673